LETTER

doi:10.1038/nature10581

Reconstructed changes in Arctic sea ice over the past 1,450 years

Christophe Kinnard[1], Christian M. Zdanowicz[2], David A. Fisher[2], Elisabeth Isaksson[3], Anne de Vernal[4] & Lonnie G. Thompson[5]

Arctic sea ice extent is now more than two million square kilometres less than it was in the late twentieth century, with important consequences for the climate, the ocean and traditional lifestyles in the Arctic[1,2]. Although observations show a more or less continuous decline for the past four or five decades[3,4], there are few long-term records with which to assess natural sea ice variability. Until now, the question of whether or not current trends are potentially anomalous[5] has therefore remained unanswerable. Here we use a network of high-resolution terrestrial proxies from the circum-Arctic region to reconstruct past extents of summer sea ice, and show that—although extensive uncertainties remain, especially before the sixteenth century—both the duration and magnitude of the current decline in sea ice seem to be unprecedented for the past 1,450 years. Enhanced advection of warm Atlantic water to the Arctic[6] seems to be the main factor driving the decline of sea ice extent on multidecadal timescales, and may result from nonlinear feedbacks between sea ice and the Atlantic meridional overturning circulation. These results reinforce the assertion that sea ice is an active component of Arctic climate variability and that the recent decrease in summer Arctic sea ice is consistent with anthropogenically forced warming.

Sea ice cover in the Arctic has been steadily decreasing over recent decades, with record losses in recent years[1,2]. The late-summer ice cover, mainly composed of thick multi-year ice, has been shrinking the fastest (−8.6% per decade)[4], which may soon result in an ice-free Arctic Ocean[7]. The loss of sea ice is having, and will continue to have, profound repercussions on the climate, ocean circulation, ecology and economics of the Arctic[2]. The short period of historical and satellite observations (about 100 years) hampers our understanding of natural variability of sea ice, so that longer time series are much needed to place recent trends in a long-term context. Although a few multi-centennial records exist in the European Arctic[5], full hemispheric coverage began only in the late nineteenth century[3]. Here we present a reconstruction of variability in sea ice cover in the Arctic over the past 1,450 years based on a network of high-resolution climate proxy records from the circumpolar region. Our proxy-based reconstruction is compared with other temperature and atmospheric circulation reconstructions and indices to identify natural drivers of variability in sea ice in pre-industrial times.

Sea ice cover is thermodynamically and dynamically controlled by both the atmosphere and the ocean. A proxy-based reconstruction should therefore include atmospheric as well as oceanic proxies (such as water temperature or salinity). Unfortunately there are currently very few oceanic proxy records of sea ice cover with high (less than 10-year) temporal resolution[5,8,9]. Alternatively, terrestrial archives can be used to document the atmospheric forcing of, or atmospheric response to, changes in sea ice cover[5,10,11]. Ice cores preserve signals of atmospheric temperature, moisture source and marine aerosol loadings, all of which may be linked to sea ice conditions[11,12]. Similarly, tree-ring and lake sediments from circum-Arctic sites reflect coastal summer climate conditions[13], which may also be linked to sea ice cover[14]. In this study we used a combination of these records to reconstruct variability in Arctic sea ice cover at a five-year resolution since AD 561. We used partial least-square (PLS) regression[15] to reconstruct the summer Arctic sea ice cover, after calibration of the multiproxy network against observational sea ice data over the late nineteenth and twentieth centuries. This approach is founded on the assumption that a component of the temporal covariance of the proxy network is related to the extent of Arctic sea ice cover, and that the relationships between individual proxies and sea ice cover were the same during and before the calibration period. These methods are widely applied for hemispheric-scale palaeoclimate reconstructions, and their merits and shortcomings were recently reviewed[13].

We used a circum-Arctic array of 69 proxies primarily derived from ice core records ($n = 52$), but also including some long tree-ring chronologies (11), lake sediments (4) and two historical series of sea ice observations (Fig. 1 and Supplementary Table 1). The ice-core proxies are the stable isotope ratio of oxygen ($\delta^{18}O$), an indicator of air temperature and/or water vapour source and transport history; the percentage of infiltration ice, a proxy for summer warmth, and the concentrations of sea-salt ions (Na^+ or Cl^-) and oceanic methanesulphonate, which are linked to sea ice openness and/or sea surface windiness[13]. Tree-ring widths are largely used to infer past summer temperatures, as are lake varve thicknesses[13]. Historical data include the reconstructed ice severity index for Iceland and the mean position of the August ice edge in the Barents Sea. All selected proxies have a

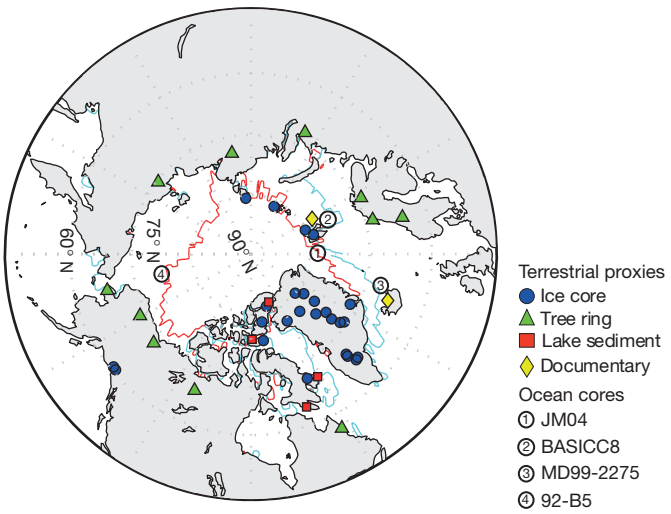

Figure 1 | Map of the Arctic showing the location and type of proxies used in the reconstruction and ocean sediment cores used for comparison. Red and blue contours respectively delineate the ice edge in August 2007 and 1951, the years of minimum and maximum ice extent from gridded historical sea ice data[3].

[1]Centro de Estudios Avanzados en Zonas Áridas, Benavente 980, Casilla 554, La Serena, 1720170, Chile. [2]Geological Survey of Canada, NRCAN, Ottawa, Ontario, K1A 0E8, Canada. [3]Norwegian Polar Institute, FRAM – High North Research Centre on Climate and the Environment, NO-9296 Tromsø, Norway. [4]GEOTOP, Université du Québec à Montréal, PO Box 8888, Montréal, Québec, H3C 3P8, Canada. [5]Byrd Polar Research Center, Ohio 43210, Columbus, USA.

time resolution better than five years. Because only terrestrial proxies are considered, coverage is poor in the central Arctic. However, sea ice variability is greatest in the marginal ice zone (the transition zone between the polar ice pack and open ocean), which is well sampled by our proxy network (Fig. 1). Many ice core records are from Greenland. This spatial heterogeneity in proxy coverage is handled by the calibration method used in the reconstruction (see Methods).

An historical index of late-summer (August) extent of Arctic sea ice (the area of the ocean with at least 15% ice concentration) was used for calibration against the proxy network over the period 1870–1995. The index integrates a gridded compilation of Northern Hemisphere sea ice data[3] with additional data coverage for the Russian Arctic obtained from a separate source[16]. The August ice extent was used because historical data from the Russian Arctic are only available for this month. The total Arctic ice extent in August is close to the September annual minimum, which corresponds approximately to the multi-year ice cover (Supplementary Fig. 1). Additional details on the historical sea ice data sets used are given in the Supplementary Information.

An exploratory Empirical Orthogonal Function (EOF) analysis was first applied on the proxy network over their common time interval, 1843–1995. Unsurprisingly, a dominant temperature-related signal was found. However, a second orthogonal mode was also revealed whose temporal variation tracked the late-summer extent of Arctic sea ice (Supplementary Figs 3 and 4 and Supplementary Information). These findings support our hypothesis that the proxy network contains an embedded climate signal specifically related to sea ice variability, which we sought to extract by using a PLS calibration approach (Methods). A skilful reconstruction of sea ice extent was possible back to AD 561 (Fig. 2a). The Reconstruction of Error skill statistic decreased from 0.84 in the most recent period to 0.43 at

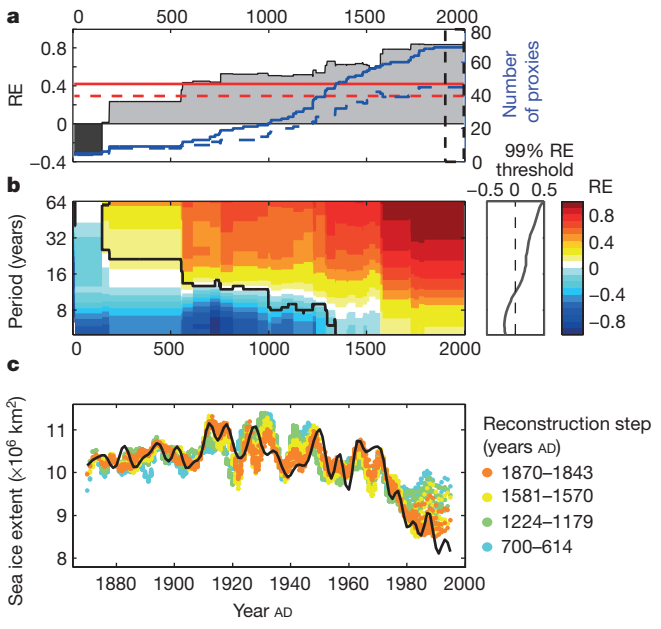

Figure 2 | Validation statistics for the reconstruction. **a**, Shaded grey/black, Reconstruction of Error (RE) statistic; continuous and dashed red lines, 99% and 95% confidence levels on RE from Monte Carlo noise simulations, respectively; blue line, number of potential proxy predictors; dashed blue line, number of proxies retained for prediction; dashed black line, calibration period 1870–1995. **b**, Multiscale validation: the black contour delineates significant RE values ($P < 0.01$); the inset shows the mean RE 99% threshold for significance by period. **c**, Observed ice extent record (black) over the 1870–1995 calibration interval and ice extent predicted by the reduced calibration sets during cross-validation, for four distinct reconstruction steps (coloured points).

AD 561, after which it became undistinguishable from chance occurrence ($P < 0.01$). Multiscale cross-validation (see Methods) shows significant positive skill at all timescales (period more than five years) after AD 1600, but prior to that, because the number of proxies decreases with increasing age, only the lower frequencies are reconstructed and with decreasing skill. At AD 561 only time periods larger than 25 years are reconstructed, with wider confidence intervals (Fig. 2b, c). A systematic bias towards overestimated reconstructed ice extent is apparent during the past 10–15 years, especially for the earlier proxy-sparse periods (Fig. 2c), which may indicate that the most recent abrupt changes in the Arctic climate system may not be fully captured by the proxies used[17].

Our proxy-based reconstructed history of late-summer Arctic sea ice extent over the period AD 561–1995 is presented in Fig. 3a along with the observed sea ice record. The reconstruction and observational record were smoothed with a 40-year lowpass filter to highlight the best-resolved frequencies (Fig. 2b). The uncertainty range around the reconstruction widens notably before about AD 1600 as a result of reduced proxy availability and consequent decrease in reconstruction skill. Within this uncertainty range, this reconstruction suggests that the pronounced decline in summer Arctic sea ice cover that began in the late twentieth century is unprecedented in both magnitude and duration when compared with the range of variability of the previous roughly 1,450 years. The most prominent feature is the extremely low ice extent observed since the mid-1990s (T1 in Fig. 3), which is well below the range of natural variability inferred by the reconstruction. Before the industrial period, periods of extensive sea ice cover occurred between AD 1200 and 1450 and between AD 1800 and 1920. Intervals of sustained low extent of sea ice cover occurred before AD 1200, and may be coincident with the so-called Medieval Warm Optimum (roughly AD 800–1300) attested in numerous Northern Hemisphere proxy records[18], but the pre-industrial minimum occurred before, at about AD 640 (T3 in Fig. 3). Two episodes of markedly reduced sea ice cover also occurred in the late sixteenth and early seventeenth centuries (T2 in Fig. 3). However, by the mid-1990s the observed decrease in sea ice cover had exceeded the lower 95% confidence limit of these pre-historical minima. Our findings support a previous study suggesting that the impact of anthropogenic climate warming on Arctic sea ice became detectable from the early 1990s onwards[19]. The present decline in sea ice is occurring at a pace seen in earlier episodes, but the sustained trend (now nearly 50 years long) is unprecedented in the 1,450-year reconstruction period presented here.

We compared our reconstruction of late-summer sea ice cover derived from terrestrial proxies with independent proxy records of regional sea ice conditions derived from ocean sediment cores. Records for the seasonal duration of sea ice in the Chukchi Sea[9] (Fig. 3b) and Fram Strait[20] (Fig. 3c), reconstructed from dinocyst assemblages, share some of the temporal features of our reconstruction, in particular a pre-industrial minimum around AD 640 in Fram Strait (T3 in Fig. 3), and an apparently marked decrease in sea ice cover between AD 1450 and 1620 in both the Fram Strait and Chukchi Sea (T2 in Fig. 3). Other dinocyst records from northern Baffin Bay and the Beaufort Sea in the Canadian Arctic also show a sea ice minimum around AD 1600 (ref. 21). However, a more detailed comparison is impossible, given the relatively coarse temporal resolution (15–100 years) of oceanic records. The similarity between our Arctic-wide sea ice reconstruction and the dinocyst-based record from Fram Strait suggests that this area, which represents the main connective pathway between the Arctic and the mid latitudes[2,22], had a key role in Arctic-wide variations in sea ice extent at interdecadal timescales. Sea ice occurrence in the Barents Sea (Fig. 3d) and in northern Iceland (Fig. 3e) was reconstructed from the sea ice biomarker IP25, which reflects springtime conditions when diatoms bloom[8,23]. The Barents Sea record shows similarities to our Arctic-wide reconstruction and the other records: low values at AD 1600, an increase afterwards and a minimum in the late twentieth century. The record from northern

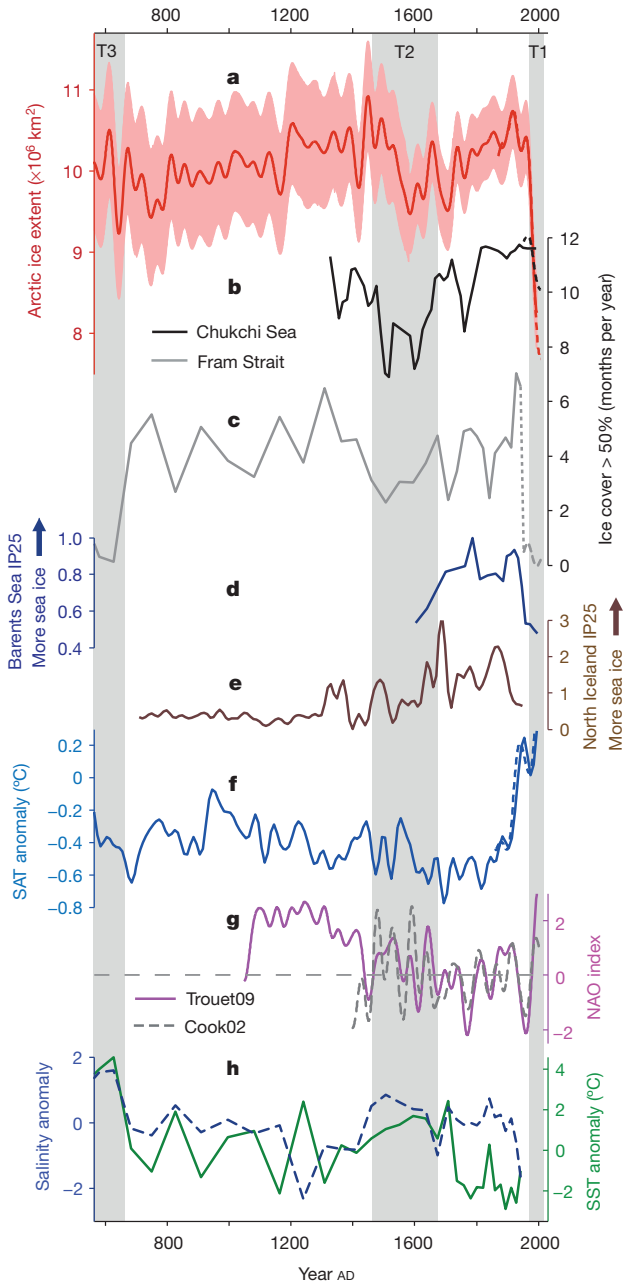

Figure 3 | Comparison between reconstructed late-summer Arctic ice extent and other Arctic sea ice, climate and oceanic proxy records. **a**, Forty-year smoothed reconstructed late-summer Arctic sea ice extent with 95% confidence interval. **b**, Chukchi Sea ice cover duration reconstructed from core 92-B5 (ref. 9). **c**, Fram Strait sea ice cover duration reconstructed from core JM04 (ref. 20). **d**, Normalized IP25 flux in the BASICC-8 sediment core, a proxy for springtime sea ice occurrence in the western Barents Sea. The timescale used is the average of the two published timescales, corresponding to high and low sedimentation rate alternatives[23]. **e**, Relative abundance of IP25 in core MD99-2275, a proxy for springtime sea ice occurrence along the northern coast of Iceland[8]. **f**, Reconstructed Arctic surface air temperature anomalies[24]. Our sea ice reconstruction includes 9 of the 23 proxies used in this reconstruction. **g**, Two reconstructions of the NAO index[25,26]. The Cook02 record mainly reconstructs interannual variations[26]; its variance was matched to the Trouet09 record, which reflects decadal-scale changes[25]. **h**, Reconstructed sea surface temperature (SST) and salinity in Fram Strait[20]. All records with a time resolution smaller than 40 years were interpolated to 1 year and then smoothed with a 40-year lowpass filter. The dashed lines in **a**, **b**, **c** and **f** are from modern observations. The dotted line in **c** is interpolated between modern observations and the reconstruction. The shaded grey areas T1–T3 delineate the periods of reduced ice extent discussed in the text.

Iceland differs somewhat from the other reconstructions, with a markedly low incidence of sea ice before AD 1200 and a general increase afterwards (Fig. 3e). Accordingly, the Iceland ice severity index is well correlated with the Iceland IP25 record[8], but not with the Arctic-wide historical ice extent record, and it has a small weight in the reconstruction (Supplementary Table 1). The occurrence of sea ice along the Icelandic coast during winter and spring partly reflects sea ice advection (drift) out of the Arctic rather than ice edge position and sea ice extent.

To evaluate the influence of temperature and dynamic (circulation) forcings on Arctic sea ice extent, we compared our 1,450-year sea ice history with proxy-based reconstructions of Arctic surface atmospheric temperatures (SATs)[24] and of the North Atlantic Oscillation (NAO) index[25,26]. The SAT record shows a sustained cooling trend over about the past 1,250 years followed by an abrupt and pronounced warming in the twentieth century (Fig. 3f). The NAO index also decreased from about AD 1100 onwards, with recent (positive) index values rising sharply in the mid-twentieth century (Fig. 3g). Although the cooling SAT trend is matched by increasing ice extent before AD 1450, both records are otherwise poorly correlated ($r = -0.12$). This reinforces our view that the proxy-based sea ice reconstruction is not just another surrogate Arctic temperature history but instead captures a sea-ice-related climate signal that is not uniquely driven by changes in SATs. Our reconstructed sea ice history is also poorly correlated with the reconstructed NAO indices (Trouet09, $r = 0.03$; Cook02, $r = -0.13$). Hence, the anticorrelation between Arctic sea ice cover and the NAO and related Arctic Oscillation (AO) index reported for recent decades[22] is not readily apparent over the extended sea ice reconstruction. These comparisons suggest that, over the past 1,450 years, changes in the summer extent of Arctic sea ice were not solely forced by SATs or by the NAO/AO, but more probably by a combination of these (and/or other) forcings.

The pronounced decrease in ice cover observed in both our terrestrial and oceanic proxy-based reconstructions between the late fifteenth and early seventeenth centuries occurred during the widespread cooling period known as the Little Ice Age (about AD 1450–1850 (ref. 18)). Reconstructed Arctic SATs show episodes of warming during this period (Fig. 3f), but according to our results the decrease in Arctic sea ice extent during the Little Ice Age was more pronounced than during the earlier Medieval Warm Optimum. A recent climate model simulation of the fifteenth-century Arctic warming (about AD 1470–1520) suggests that it could have been solely driven by enhanced southerly advection of warm air into the Arctic[27]. This is not evident from the reconstructed NAO indices, which alternate between positive and negative and hence do not indicate a markedly increased meridional atmospheric circulation at that time (Fig. 3g). In contrast, positive, synchronous sea surface temperature and salinity anomalies in Fram Strait during this period inferred from dinocyst assemblages (Fig. 3h) suggest increased advection of warm and saline water from the North Atlantic into the Arctic Ocean[20], and this could have accounted for a decrease in sea ice cover in the Arctic Ocean. Similarly, the pre-industrial minimum in sea ice cover at about AD 640 occurred at the beginning of the Dark Age Cold Period (about AD 600–900 (ref. 28)) under overall cold conditions but was accompanied by increased northward advection of Atlantic water (Fig. 3h). These observations suggest that at multidecadal to centennial timescales, the Arctic sea ice cover during the pre-industrial period may have varied primarily in response to the advection of warm Atlantic water into the Arctic, perhaps as part of internal coupled ocean–atmosphere–sea ice oscillations[29]. Similarly, heat transfer to the Arctic by warm Atlantic water has been shown recently to be unprecedented over the past 2,000 years[28] and may be the main driver for the sustained loss of Arctic sea ice over recent decades. In the present state of knowledge, anthropogenically forced ('greenhouse gases') warming stands out as a very plausible cause of the record atmospheric and oceanic warmth of the recent decades, which may soon lead to an ice-free Arctic Ocean in summer.

METHODS SUMMARY

We used PLS regression, a multivariate calibration method widely used in analytical chemistry[15], to calibrate the multiproxy ensemble against modern observations of sea ice. The PLS method uses an iterative procedure to generate a set of orthogonal vectors (scores), which are linear combinations of the predictor variables (proxies) and have maximum covariance with the predictand vector (ice extent). PLS constitutes a more flexible approach in our case in which sea ice is not the dominant signal in the proxy network, and it is also ideally suited to deal with a large spatial array of collinear predictor variables, because it permits spatially clustered and/or collinear variables to be combined into fewer vector(s). To account for the uneven number of proxies over time, we used a 'stepwise' calibration approach[17,26], in which new PLS models were constructed as an increasing number of proxies become available over time. For each model a proxy selection algorithm chose the best subset of predictors based on the available proxies and their contribution to the prediction skill (Methods). At most, 45 proxies were used as predictors in the most recent period, and a minimum of eight proxies were used in the last segment of the reconstruction (Fig. 2a). Model skill was estimated by moving block cross-validation. The Reduction of Error statistic, which predominantly measures the low-frequency skill of a reconstruction[30], was used as the prediction skill diagnostic as in previous studies[17,26,30]. We also introduced a multiscale validation procedure to assess the predictive skill of each PLS model at different timescales, by applying cross-validation at separate frequency bands (Supplementary Information). The statistical significance of the model prediction skill was determined by Monte Carlo simulations with auto-correlated noise (Methods).

Full Methods and any associated references are available in the online version of the paper at www.nature.com/nature.

Received 24 December 2010; accepted 21 September 2011.

1. Serreze, M. C., Holland, M. M. & Stroeve, J. Perspectives on the Arctic's shrinking sea-ice cover. *Science* **315,** 1533–1536 (2007).
2. Perovich, D. & Richter-Menge, J. Loss of sea ice in the Arctic. *Annu. Rev. Mar. Sci.* **1,** 417–441 (2009).
3. Walsh, J. E. & Chapman, W. L. 20th-century sea-ice variations from observational data. *Ann. Glaciol.* **33,** 444–448 (2001).
4. Comiso, J. & Nishio, F. Trends in the sea ice cover using enhanced and compatible AMSR-E, SSM/I, and SMMR data. *J. Geophys. Res.* **113,** doi:10.1029/2007JC004257 (2008).
5. Polyak, L. *et al.* History of sea ice in the Arctic. *Quat. Sci. Rev.* **29,** 1757–1778 (2010).
6. Spielhagen, R. F. *et al.* Enhanced modern heat transfer to the Arctic by warm Atlantic water. *Science* **331,** 450–453 (2011).
7. Wang, M. & Overland, J. A sea ice free summer Arctic within 30 years. *Geophys. Res. Lett.* **36,** L07502, doi:10.1029/2009GL037820 (2009).
8. Massé, G. *et al.* Abrupt climate changes for Iceland during the last millennium: evidence from high resolution sea ice reconstructions. *Earth Planet. Sci. Lett.* **269,** 565–569 (2008).
9. de Vernal, A., Hillaire-Marcel, C., Solignac, S., Radi, T. & Rochon, A. in *Arctic Sea Ice Decline: Observations, Projections, Mechanisms, and Implications* (eds DeWeaver, E. T., Bitz, C. M. & Tremblay, L.-B.) (Geophysical Monograph Series Vol. 80) 27–45 (American Geophysical Union, 2008).
10. Macias Fauria, M. *et al.* Unprecedented low twentieth century winter sea ice extent in the Western Nordic Seas since AD 1200. *Clim. Dyn.* **34,** 781–795 (2010).
11. Fisher, D. *et al.* Natural variability of Arctic sea ice over the Holocene. *Eos* **87,** 273–275 (2006).
12. Grumet, N. S. *et al.* Variability of sea-ice extent in Baffin Bay over the last millennium. *Clim. Change* **49,** 129–145 (2001).
13. Jones, P. D. *et al.* High-resolution palaeoclimatology of the last millennium: a review of current status and future prospects. *Holocene* **19,** 3–49 (2009).
14. Jacoby, G. C. & Ulan, L. D. Reconstruction of past ice conditions in a Hudson Bay estuary using tree rings. *Nature* **298,** 637–639 (1982).
15. Wold, S., Sjöström, M. & Eriksson, L. PLS-regression: a basic tool of chemometrics. *Chemom. Intell. Lab. Syst.* **58,** 109–130 (2001).
16. Polyakov, I. *et al.* Long-term ice variability in Arctic marginal seas. *J. Clim.* **16,** 2078–2085 (2003).
17. Mann, M. E. *et al.* Proxy-based reconstructions of hemispheric and global surface temperature variations over the past two millennia. *Proc. Natl Acad. Sci. USA* **105,** 13252–13257 (2008).
18. Jones, P. & Mann, M. Climate over past millennia. *Rev. Geophys.* **42,** RG2002, doi:10.1029/2003RG000143 (2004).
19. Min, S.-K., Zhang, X., Zwiers, F. W. & Agnew, T. Human influence on Arctic sea ice detectable from early 1990s onwards. *Geophys. Res. Lett.* **35,** doi:10.1029/2008GL035725 (2008).
20. Bonnet, S., de Vernal, A., Hillaire-Marcel, C., Radi, T. & Husum, K. Variability of sea-surface temperature and sea-ice cover in the Fram Strait over the last two millennia. *Mar. Micropaleontol.* **74,** 59–74 (2010).
21. Richerol, T. *et al.* Evolution of paleo sea-surface conditions over the last 600 years in the Mackenzie Trough, Beaufort Sea (Canada). *Mar. Micropaleontol.* **68,** 6–20 (2008).
22. Dickson, R. *et al.* The Arctic Ocean response to the North Atlantic Oscillation. *J. Clim.* **13,** 2671–2696 (2000).
23. Vare, L. L., Massé, G. & Belt, S. T. A biomarker-based reconstruction of sea ice conditions for the Barents Sea in recent centuries. *Holocene* **20,** 637–643 (2010).
24. Kaufman, D. *et al.* Recent warming reverses long-term Arctic cooling. *Science* **325,** 1236–1239 (2009).
25. Trouet, V. *et al.* Persistent positive North Atlantic Oscillation mode dominated the medieval climate anomaly. *Science* **324,** 78–80 (2009).
26. Cook, E. R., D'Arrigo, R. D. & Mann, M. E. A well-verified, multiproxy reconstruction of the winter North Atlantic Oscillation index since A.D. 1400. *J. Clim.* **15,** 1754–1764 (2002).
27. Crespin, E., Goosse, H., Fichefet, T. & Mann, M. The 15th century Arctic warming in coupled model simulations with data assimilation. *Clim. Past* **5,** 389–401 (2009).
28. Spielhagen, R. F. *et al.* Enhanced modern heat transfer to the Arctic by warm Atlantic water. *Science* **331,** 450–453 (2011).
29. Holland, M. M., Bitz, C. M., Eby, M. & Weaver, A. J. The role of ice-ocean interactions in the variability of the North Atlantic thermohaline circulation. *J. Clim.* **14,** 656–675 (2001).
30. Wahl, E. & Ammann, C. Robustness of the Mann, Bradley, Hughes reconstruction of Northern Hemisphere surface temperatures: examination of criticisms based on the nature and processing of proxy climate evidence. *Clim. Change* **85,** 33–69 (2007).

Supplementary Information is linked to the online version of the paper at www.nature.com/nature.

Acknowledgements This work was supported jointly by the Canadian Foundation for Climate and Atmospheric Sciences (Polar Climate Stability Network) and the Natural Sciences and Engineering Research Council of Canada.

Author Contributions C.K. conducted all data preparation and analyses. C.M.Z. and D.A.F. instigated and directed the research and contributed to the interpretation. E.I., A.deV. and L.G.T. contributed data and participated in the interpretation of results. All authors contributed to manuscript preparation.

Author Information Reprints and permissions information is available at www.nature.com/reprints. The authors declare no competing financial interests. Readers are welcome to comment on the online version of this article at www.nature.com/nature. Correspondence and requests for materials should be addressed to C.K. (christophe.kinnard@ceaza.cl).

METHODS

Proxies pre-processing. The year 1995, beyond which many proxies terminate, was chosen as the end point for the calibration interval. Proxies with missing values in the 1870–1995 calibration interval were filled on the basis of their covariance with the other proxy records, using an EOF-based data-filling procedure[31] (Supplementary Information). All proxies were interpolated to a resolution of 1 year then smoothed to 5-year resolution with a lowpass filter. Extreme proxy values (± 4 s.d. around the mean) were deleted and interpolated linearly. Both the proxies and the sea ice series were mean-centred over the calibration interval, and the proxies were also standardized to unit variance over the same interval.

Calibration methods. Various methods have been used to calibrate climate observations against a multiproxy network, ranging from simple compositing and variance scaling (CPS), to multivariate climate field reconstructions (CFR)[13,32–34]. In our case, because sea ice cover is not the dominant signal in the proxy network, a simple CPS approach could not be used. PLS regression[15,35] was used to calibrate observations of sea ice extent with the proxy network. A small number of PLS vectors is usually retained to model the predictand and to guard against statistical overfitting. PLS is similar to Canonical Regression[36] and Principal Component Regression (PCR) used in previous palaeoclimate reconstructions[26,36,37]. However, in PLS, vectors are computed and ranked by their covariance with the predictand series, whereas in PCR the vectors are determined solely by the covariance between the predictors, using EOF. The number of potential predictors (proxies) k decreased back in time, from 69 in AD 1995 to 12 at AD 561 (Fig.2a). The calibration was performed over the period 1870–1995 ($n = 126$ years) using a 'stepwise' approach[17,26,37], in which new PLS models were constructed as an increasing number of proxies become available over time. PLS projects the predictor matrix X (the proxies) into a set of orthogonal score vectors t that successively maximize the covariance with the dependent variable y (sea ice extent). A reduced number of scores, $a < k$, is retained for the prediction of y. The PLS model for a single predictand variable is expressed by

$$X = TP' + E$$

$$y = Tq' + f$$

where $T\,[n \times a]$ is the score matrix; $P\,[k \times a]$ is the loading matrix of X; $E\,[n \times k]$ is the residual matrix of X; q is the loading matrix of y and $f\,[n \times 1]$ is the vector of y residuals. The matrix transpose is expressed by the prime symbol. The PLS scores and loadings are calculated successively using the Nonlinear Iterative Partial Least Square (NIPALS) algorithm. For a single predictand variable y, the NIPALS algorithm is as follows:

(1) Compute a vector of weights $w = X'y/(y'y)$.
(2) Normalize the weights vector $w = w/||w||$ (Euclidean norm).
(3) Calculate the score vector $t = Xw$.
(4) Calculate the loadings for X and y as $P = X't/(t't)$ and $q = y't/(t't)$.
(5) The residuals f in y are given by $f = y - tq'$.
(6) The deflated (residual) matrix of predictors is $E = X - tp'$.

Each consecutive component $(1, \ldots, a)$, in the model is computed as in step 1 with $X = E$ and $y = f$, and all vectors are stored in matrices. Once the desired number of components has been calculated, the final model can be expressed by

$$\hat{y} = Xb + f$$

$$b = W(P'W)^{-1}q$$

where $b\,[k \times 1]$ is the vector of regression coefficients for a PLS model with a components and $W\,[k \times a]$ is the weight matrix of X.

Model validation. Because of its strong persistence and relatively short length ($n = 126$ years), the observed sea ice record has a low degree of freedom (about 9), which impedes discarding long segments of data for validation, as done elsewhere[17,26]. Instead, we used a moving-block strategy[38], in which all possible contiguous blocks of 15 year length were successively removed from the full data set, and PLS was applied on the reduced calibration set and validated on the excluded block. The Reduction of Error (RE) statistic, which predominantly measures the low frequency skill of a reconstruction[30], was used as the prediction skill diagnostic as in previous studies[17,26,30]. A mean RE statistic was calculated from all excluded blocks. This procedure effectively amounts to successively removing one degree of freedom from the original data before applying calibration. The block size (15 years) was estimated from the autocorrelation function of y and corresponds to the effective time between two independent observations (Supplementary Information). A backwards variable selection algorithm was incorporated in the cross-validation (CV) procedure to retain the best subset of predictors in each model[39]. A Jack-knife estimate of the variance of the PLS slope vector b was obtained from CV and the variable with the least significant contribution to the model was removed, before reapplying PLS calibration and CV until all variables retained were found to be significant. At most, 45 proxies were used as predictors in the most recent period, and a minimum of eight proxies were used in the last segment of the reconstruction (Fig. 2a). The 95% confidence interval on the reconstruction was calculated from the cross-validation residuals. We also introduce a multiscale validation procedure to assess the predictive skill of the PLS models at different timescales. The observed ice extent record as well as ice extent predicted by the perturbed PLS models (those trained on the reduced calibration sets during CV) were transformed into separate frequency bands by using the continuous wavelet transform, and a mean RE statistic was calculated at each band (Fig. 2b and Supplementary Information).

Model dimensionality. The number of PLS components a retained for the prediction of y determines the model dimensionality. Including too many components can lead to statistical over-fitting (modelling noise), whereas too few components will cause under-fitting, meaning that the model does not capture all the variability in the data. A calibration test was first applied to determine model dimensionality: the significance of the covariance between the successive y and t vectors was tested by Monte Carlo noise simulation, by randomizing the Fourier phase of y 1,000 times and calculating the product $t'y$ at each iteration. The number of components a significantly different from noise ($P < 0.1$) was retained. A validation test was also applied, by examining a plot of the root mean squared error (r.m.s.e.) calculated from cross validation as a function of a, and choosing the value a resulting in a clear minimum r.m.s.e. Both methods generally agreed, but when they differed the smallest a value was retained (Supplementary Fig. 8).

Model verification. One-tailed statistical significance tests for the prediction skill of the final PLS models were performed with the same randomization technique described above. A total of 300 surrogate proxy data sets ('nonsense predictors') were created and used to predict the record of sea ice extent, and the skill metric (RE) was calculated each time. Models with skill significantly different ($P < 0.01$) from noise were retained (Fig. 2a and Supplementary Fig. 9).

31. Beckers, J. & Rixen, M. EOF calculations and data filling from incomplete oceanographic datasets. *J. Atmos. Ocean. Technol.* **20,** 1839–1856 (2003).
32. Christiansen, B., Schmith, T. & Thejll, P. A surrogate ensemble study of climate reconstruction methods: stochasticity and robustness. *J. Clim.* **22,** 951–976 (2009).
33. Lee, T., Zwiers, F. & Tsao, M. Evaluation of proxy-based millennial reconstruction methods. *Clim. Dyn.* **31,** 263–281 (2008).
34. Mann, M. Climate over the past two millennia. *Annu. Rev. Earth Planet. Sci.* **35,** 111–136 (2007).
35. Naes, T., Isaksson, T., Fearn, T. & Davies, T. *Multivariate Calibration and Classification* (NIR Publications, 2004).
36. Cook, E., Briffa, K. & Jones, P. Spatial regression methods in dendroclimatology: a review and comparison of two techniques. *Int. J. Climatol.* **14,** 379–402 (1994).
37. Luterbacher, J., Dietrich, D., Xoplaki, E., Grosjean, M. & Wanner, H. European seasonal and annual temperature variability, trends, and extremes since 1500. *Science* **303,** 1499–1503 (2004).
38. Michaelsen, J. Cross-validation in statistical climate forecast models. *J. Appl. Meteorol.* **26,** 1589–1600 (1987).
39. Martens, H. & Martens, M. Modified Jack-knife estimation of parameter uncertainty in bilinear modelling by partial least squares regression (PLSR). *Food Qual. Prefer.* **11,** 5–16 (2000).